Available online at www.sciencedirect.com
ScienceDirect
Journal of Solid State Chemistry 179 (2006) 3718–3723
JOURNAL OF SOLID STATE CHEMISTRY
www.elsevier.com/locate/jssc

Investigation of luminescence and optical absorption of $K_2LiAlF_6:Cr^{3+}$ single crystals

M.A.F.M. da Silva[a], R.B. Barthem[b], L.P. Sosman[a,*]

[a]*Instituto de Física, Universidade do Estado do Rio de Janeiro, 20559-900, RJ, Brazil*
[b]*Instituto de Física, Universidade Federal do Rio de Janeiro, 21945-970, RJ, Brazil*

Received 14 June 2006; received in revised form 5 August 2006; accepted 7 August 2006
Available online 9 August 2006

Abstract

Photoluminescence, absorption and excitation spectra of K_2LiAlF_6 single crystals doped with 1% of Cr^{3+} are presented. The near-infrared photoluminescence observed at room temperature, 77 and 4 K are attributed to the zero-phonon spin-allowed $^4T_2(^4F) \rightarrow {}^4A_2(^4F)$ transition of Cr^{3+} octahedrally coordinated by F^- ions. Lifetimes are obtained. The 4 K emission broad band was described in terms of normal modes of the octahedral complex $[CrF_6]^{3-}$. The Racah, crystal-field and Huang–Rhys parameters are calculated and the quantum efficiency and thermal quenching estimated and compared with Cr^{3+} properties in different environments.

Keywords: Photoluminescence; Fluoride; Chromium

1. Introduction

Optical materials emitting in the visible and near infrared spectral regions have generated a strong interest due to their inherent tunability and possible applications, that include, among many others signal transmission, display devices, information storage and solid-state lasers [1–4]. Materials doped with octahedrally coordinated Cr^{3+} present wide bands originated from electronic transitions in the ionic unfilled 3*d* electronic shell. The Cr^{3+} 3*d* electrons are outside of the ion core and therefore are strongly affected by the electrostatic potential generated by ligand anions. The fundamental free-ion level of Cr^{3+} is ^{4}F. However, when the ion is on crystal host, its energy states are splited by nearby ions electrostatic field. This splitting will depend on the crystalline field intensity, defined by the *Dq* parameter, and on the electronic repulsion, defined by *B* and *C* Racah parameters. The term ^{4}F is splited into $^4A_2$ (t_2^3 electronic configuration), $^4T_2(t_2^2e)$ and $^4T_1(t_2^2e)$ energy levels. The excited free-ion level ^4P is splited into $^4T_1(t_2e^2)$. The splitting of higher ^2G level originates $^2E(t_2^3)$, $^2T_1(t_2^3)$, $^2T_2(t_2^3)$ and $^2A_1(t_2^2e)$. For Dq/B values < 2.3, the lowest excited state is $^4T_2$, whereas for Dq/B values > 2.3 the lowest excited state is the ^2E level [5]. Sharp lines are associated to transitions between levels that belong to same electronic configurations and broad bands are attributed to transitions between states that present different electronic configurations.

Until today the most efficient solid-state laser is the $Be_3Al_2(SiO_3)_6:Cr^{3+}$, emitting between 720 and 849 nm with intensity peak at 768 nm and efficiency of 0.64 [6], followed by $LiCaAlF_6:Cr^{3+}$ laser, with emission also between 720 and 840 nm, maximum intensity at 780 nm and efficiency of 0.54 [7]. Systems with wider emissions are the $LiSrAlF_6:Cr^{3+}$, emitting between 780 and 1010 nm with maximum at 825 nm and efficiency of 0.36 [8] and the $La_3Ga_5SiO_{14}:Cr^{3+}$, tunable between 862 and 1107 nm with peak at 968 nm, but with only 0.10 of efficiency [9]. As can be seen, obtaining a new material with emission located under 700 nm, in the visible range, would be interesting. Fluoride compounds doped with transition metal ions have been reported in the literature [10–13], and it is now well established that they present long upper-state lifetimes, and

*Corresponding author. Fax: +55 21 25877447.
E-mail addresses: sosman@uerj.br, lpsosman@uerj.br (L.P. Sosman).

0022-4596/$ - see front matter © 2006 Elsevier Inc. All rights reserved.
doi:10.1016/j.jssc.2006.08.003

are, consequently, potential materials to be used as efficient amplifying media. Moreover, the observation of a broad red absorption bands allows direct diode pumping. Therefore our interest is the optical characterization of the fluoride $K_2LiAlF_6:Cr^{3+}$, through luminescence and absorption techniques, in order to verify its possible application as a tunable laser material.

The fluoride K_2LiAlF_6 is an A_2BMX_6 material, where A and B are monovalent alkali metals, M is a trivalent metal and X is a monovalent anion. In K_2LiAlF_6 the tolerance factor $t = 1$ indicate a hexagonal perovskites or elpasolite structure rather than cubic [14], and the symmetry was reported formerly as hexagonal rhombohedral $R\bar{3}m$ space group, with lattice parameters $a = 5.62 \pm 0.01$ Å and $c = 27.62 \pm 0.01$ Å of hexagonal cell [15]. The K_2LiAlF_6 framework, as we can see in Fig. 1, presents a group of three octahedra interconnected through faces, with three M (Al^{3+}, Li^{+}) and 12 F^{-} ions. The central octahedrally coordinated position is occupied by Al^{3+} ion while Li^{+} ions occupy the two external ones. This group is connected with another similar trimeric group through AlF_6 octahedra. The MF_{12} and AlF_6 share a corner [15]. With this ions distribution it is expected that dopant Cr^{3+} ions remain octahedrally surrounded by F^{-} anions in the host lattice. Actually, K_2LiAlF_6 optical measurements indicate that Cr^{3+} ions are octahedrally coordinated and replace the host Al^{3+} occupying only one kind of site. In addition, from the emission spectra measured at 4, 77 K and room temperature and from absorption and excitation spectra measured at room temperature, we could assign the energy levels of the chromium ion in the host material. From the room temperature excitation spectrum we calculated the value of $Dq/B = 2.3$. This value indicates that the energy levels of the $^4T_2(^4F)$ and $^2E(^2G)$ are very close to each other but the lowest excited state is $^4T_2$. The luminescence was attributed to $^4T_2 \rightarrow {}^4A_2$ transition and the calculated Huang–Rhys factor $S = 2.4$ is compatible with the emission assignment [5].

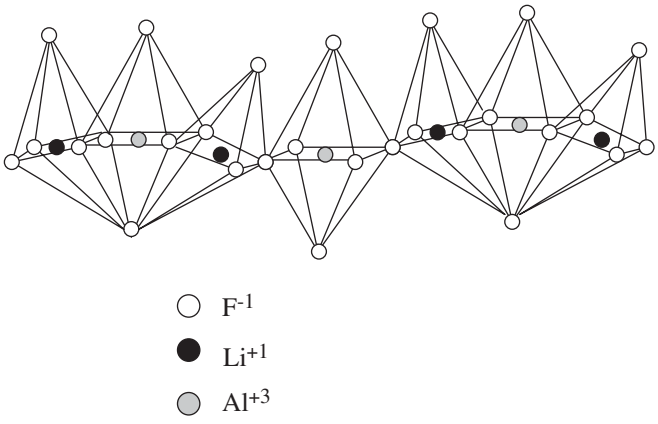

Fig. 1. K_2LiAlF_6 framework. A group of three octahedra interconnected through faces, with three M (Al^{3+}, Li^{+}) and 12 F^{-} ions is connected with another similar trimeric group sharing a corner AlF_6 octahedra.

2. Experimental details

Luminescence, absorption and excitation spectra were obtained with a 2061 McPherson spectrometer to scan the emission, a RCA 31034 photomultiplier and an AM505F ARC spectrometer to select the excitation wavelength. The exciting sources were a 250 W tungsten lamp and a cw 488 nm line from a Laser Ion Technology Ar-ion laser model 5400-220-00. The excitation intensity was modulated at a reference frequency using a PAR 191 variable speed chopper. An EG&G PAR Instrumentation model 5209 lock-in and a Tektronix Model TDS 350 digital oscilloscope were used to acquire and produce the primary signal treatment. The low-temperature experiments were performed using a Janis ST-100 gas flow cryostat. All the spectra were corrected for the response of the monochromator and detection system.

$K_2LiAlF_6:Cr^{3+}$ single crystals up to 0.5 cm^3 in size were grown by the hydrothermal method with 1.0% of Cr^{3+} ion as impurity [16]. The obtained crystal phase homogeneity and the possible distortions of crystal lattice were tested by the X-ray powder diffraction method. The ionic radius of Al^{3+} and Cr^{3+} are, respectively, 0.57 and 0.64 Å, while the ionic radius of K^{+} is 1.33 Å and of Li^{+} is 0.78 Å. By looking exclusively to the ionic radius, it is possible an occupation of Li^{+} or Al^{3+} sites by Cr^{3+} ions, due the proximity of ionic radius values. But, Li^{+} and Cr^{3+} ionic valences are different, so this substitution would cause a great change in atomic positions to compensate charges. For this reason, together with close values for the host-impurity ionic radius, the same valence of host and a substitutional ion is an important factor. Therefore, despite that the ratio $r_{Al^{3+}}/r_{Cr^{3+}} \sim 0.9$ can produce additional distortions in host structure, the Cr^{3+} ions enter into the host replacing the Al^{3+} ions without charge compensation. Due to the low level of doping, we can suppose that changes in host structure for the Cr^{3+} site occupation should be very low.

3. Results and discussion

The K_2LiAlF_6 luminescence spectra containing 1.0% of Cr^{3+} at room temperature, 77 and 4 K are shown in Fig. 2(a)–(c), respectively. These spectra were obtained with a 488 nm Ar-ion laser excitation wavelength. At room temperature (Fig. 2(a)) we can observe the emission band between 650 and 850 nm with barycenter at 735 nm. In the Cr^{3+} spectra, sharp lines are associated to transitions between levels of same electronic configurations and broad bands are attributed to transitions between states that present different electronic configurations. The $^4T_2$ state has a t_2^2e electronic configuration, while the $^4A_2$ and ^2E states have t_2^3 configuration. Therefore the observed broad emission bands are identified as the phonon assisted $^4T_2(^4F) \rightarrow {}^4A_2(^4F)$ electronic transition of the forbidden d–d crystal field levels of Cr^{3+} ions in octahedral sites [17]. The lifetime measured through the phase shift method was

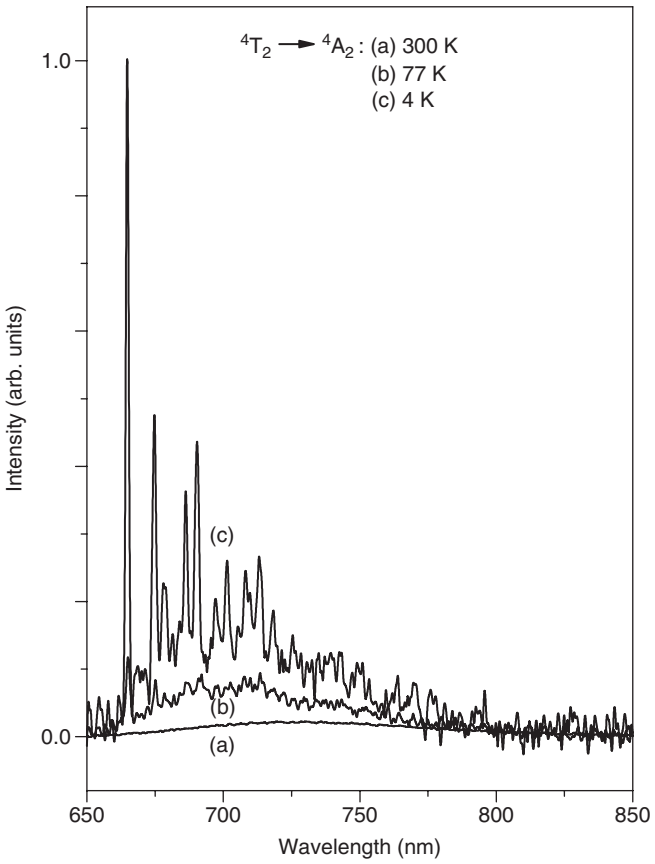

Fig. 2. Photoluminescence spectra of K_2LiAlF_6 doped with 1.0 at% Cr^{3+} at: (a) room temperature (300 K), (b) 77 K and (c) 4 K. At RT the luminescence lifetime measured through the phase-sensitive detection was $\tau_{300\,K} = 567\,\mu s$, while $\tau_{4\,K} \sim 1.7\tau_{300\,K}$. These close values are an indication that the Cr^{3+} ions occupy undistinguishable octahedral sites in the host structure.

$\tau_{300\,K} = 570\,\mu s$. This decay time is an average value, because it was not possible to verify the existence of two or more different occupation sites for the Cr^{3+} ions. The 77 K emission spectrum, Fig. 2(b), exhibits a broad band also located between 650 and 850 nm, but with barycenter at 708 nm and a number of weaker emissions. The luminescence spectrum at 4 K is shown in Fig. 2(c). The emission exhibits an intense line at 664.7 nm (15,044 cm^{-1}) with luminescence lifetime $\tau_{4\,K} = 980\,\mu s$ and very rich fine structure, superposed to a broad vibronic one. This lifetime differs only by a factor of 1.7 from $\tau_{300\,K}$, indicating that the emission at 4 K can also be associated to the $^4T_2(^4F) \rightarrow {}^4A_2(^4F)$ transition. It is commonly recognized that Cr^{3+} in intermediate crystalline field can present emissions from the level ^2E [18–20]. Therefore, in order to distinguish the different transitions for other probable Cr^{3+} sites, we choose appropriates phases in lock-in amplifier that eliminates the line at 664.7 nm. But this procedure eliminates all the others lines in the spectrum. Obviously, we conclude that all lines present very close lifetimes, pointing out that the Cr^{3+} ions occupy undistinguished octahedral sites in the host structure and only $^4T_2(^4F) \rightarrow {}^4A_2(^4F)$ transition can be ascribed with observed luminescence. Moreover, the similar energy position, the band shape, as well as the value of the measured lifetimes, also indicate that spectra at room temperature, 77 and 4 K have the same the $^4T_2$ level origin of isolated impurity centers.

Assuming that luminescence temperature quenching is only due to non-radiative decays and considering the emission quantum efficiency at 4 K as 100%, the transition quantum efficiency at room temperature (ϕ) could be estimated from the ratio $\phi = \tau_{300\,K}/\tau_{4\,K}$ [1,3]. For room temperature this shows a Cr^{3+} emission quantum efficiency of approximately 0.6. It can be seen from Fig. 2 that the luminescence intensity strongly decreases with temperature increasing. Only 10% of the 4 K-emission integrated intensity remains at room temperature. Certainly non-radiative decay processes are the only responsible because, for low dopant ion concentration in studied samples, it would not be expected an energy transfer between Cr^{3+} ions. The correlation between observed quenching of the emission and the Stokes shift will be argued later.

The assignment of luminescence spectra can be confirmed by Huang–Rhys parameter S. When the first excited level is $^4T_2$ the electron–lattice coupling is strong and S value is higher than 1, while for $S<1$ the coupling is weak and the luminescent emission is from ^2E level. From Fig. 2, we calculate the S factor, with $e^{-S} = I_{ZPL}/I$ [1], where I and I_{ZPL} are the integrated intensity in the broadband and zero-phonon line, respectively. For K_2LiAlF_6:Cr^{3+} this parameter was found to be 2.4, compatible with the $^4T_2(^4F) \rightarrow {}^4A_2\,(^4F)$ assignment.

Details of the luminescence spectrum at 4 K are shown in Fig. 3. The low temperature $^4T_2(^4F) \rightarrow {}^4A_2(^4F)$ emission exhibits a very rich fine structure, superposed to a broad vibronic band that extends from 650.0 to 850.0 nm. In Cr^{3+}-fluoride host, the chromium wave functions overlap those of the six F^- nearly surrounding neighbors. This overlapping is simply represented by the combination of the Cr^{3+} plus the F^- contributions to the molecular orbital for the $[CrF_6]^{3-}$ octahedral complex. The Cr^{3+} orbitals are s, p and d while F^- orbitals are s and p. The overlapping of p and d orbitals is responsible by the formation of π molecular orbitals. However, the combination of s, p and d orbitals produces σ molecular orbitals, which present higher stability than π orbitals [21]. Orbitals σ are symmetric with respect to a rotation around the bond direction while π orbitals are not symmetric. The transformation of atomic orbitals results in four chromium orbitals $3d$ (t_{2g}, e_g), $4s$ (a_{1g}) and $4p$ (t_{1u}) and seven fluorine orbitals, $2p_\sigma$ (a_{1g}, t_{1u}, e_g) and $2p_\pi$ (t_{1u}, t_{2g}, t_{2u}, t_{1g}). Therefore, the structure observed in 4 K luminescence spectrum was analyzed in terms of the normal modes of vibration of $[CrF_6]^{3-}$ octahedral complex based on molecular orbital theory. In Fig. 3, we can clearly observe the zero-phonon line located at 664.7 nm (15,044 cm^{-1}), line 1, and vibrational lines associated with the $^4T_2(^4F) \rightarrow {}^4A_2(^4F)$ transition, where the signal phase was adjusted to obtain

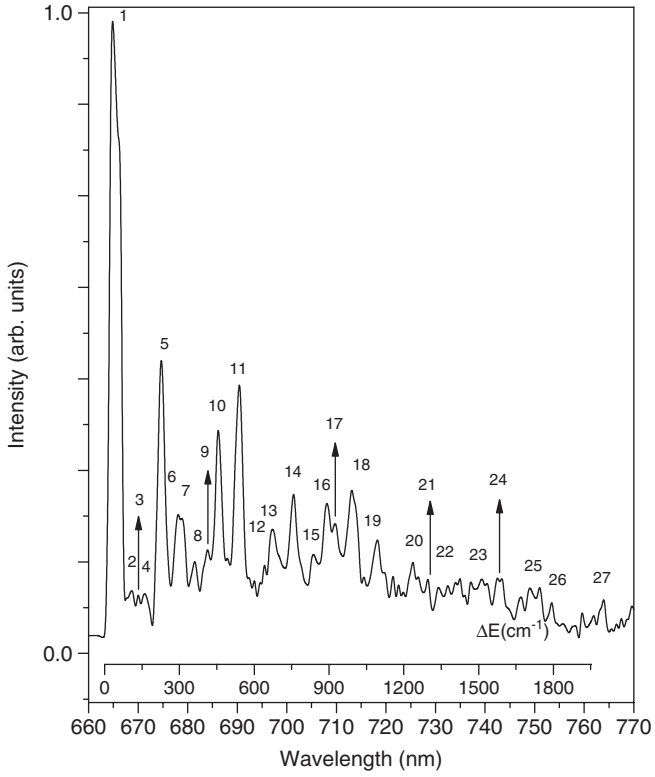

Fig. 3. Detailed photoluminescence spectrum of K_2LiAlF_6 doped with 1.0 at% Cr^{3+} at 4 K. The zero-phonon, located at 15044 cm^{-1}, is indexed as line 1.

the maximum intensity for line 1. It is clear that, in perfectly octahedral coordination sites, the parity forbidden *d–d* transitions are of magnetic dipole (MD). But MD transitions originate weak lines in optical spectra. As we can observe in Fig. 3, the K_2LiAlF_6:Cr^{3+} spectrum presents several intense lines. However, stronger intensity line is characteristic of electronic dipole (ED) transitions that occur only in Cr^{3+} sites without inversion of symmetry. From this we conclude that actually Cr^{3+} ions occupy sites in host lattice in which the symmetry is reduced below octahedral, due to ratio $r_{Al}^{3+}/r_{Cr}^{3+}<1$. Therefore the emission spectrum is dominated by electric dipole vibronic band [22]. The very small 2–4 lines at 668.6, 670.1 and 671.3 nm appear for the lattice vibrations. We can now analyze briefly the other intense side lines. The line 5 located at 674.7 nm is associated with energy transition produced by an odd-parity internal vibration of the complex $[CrF_6]^{3-}$, namely the $t_{2u}(\pi)$ bending mode. The weaker $t_{2g}(\pi)$ mode [2,23] at 676.2 nm was assumed successfully as a component on the low energy side of higher intensity $t_{2u}(\pi)$ mode after some failed previous attempts of assignments of longer wavelength modes. The sensibility of the detection system is also determinant for the apparent absence of the $t_{2g}(\pi)$ mode. Following the more intense spectral lines, three vibronic peaks situated at 678.3, 686.2 and 690.4 nm, identified in the spectrum as 7, 10 and 11 lines, can be assigned, respectively, as $t_{1u}(\pi)$ bending mode, $e_g(\sigma)$ and $a_{1g}(\sigma)$ stretching modes. For Cr^{3+} systems in which $^4T_2$ and ^2E states are close, the $e_g(\sigma)$ and $a_{1g}(\sigma)$ modes are generally intense [24]. The $t_{1u}(\sigma)$ stretching mode (line 12) is located at 692.2 nm. The greater stability of σ orbitals in comparison with π orbitals is related with the energy position of the $t_{1u}(\sigma)$ mode (line 12), which is expected to lie below the $t_{1u}(\pi)$ mode (line 7). The vibrational structure assignment is in agreement with energy intervals for phonon modes in different fluorides hosts. It is expected the $t_{2u}(\pi)$ mode to be located between 160 and 220 cm^{-1}. Modes $t_{1u}(\pi)$, $e_g(\sigma)$, a_{1g} (σ) and $t_{1u}(\sigma)$ are located in the 305–335, 470–495, 555–575 and 560–590 cm^{-1} energy intervals, respectively [25]. The e_g and a_{1g} modes undergo a decrease in their energies at the same time that present higher intensities when the Cr^{3+}–F^- distance increases producing a site distortion [2,3,25]. According to this statement, the e_g and a_{1g} energy values obtained in this work point to an ion site distortion, which destroys the inversion site symmetry and produces Cr^{3+} displacement from the octahedral central position. By combining modes energy positions we identified several weak lines. The vibronic transitions for K_2LiAlF_6:Cr^{3+}, based on the zero-phonon line at 664.7 nm, are arranged in decreasing order and summarized in Table 1. The K_2LiAlF_6:Cr^{3+} vibration mode assignments are compared, in Table 2, with other fluorides hosts, in which the

Table 1
Experimental positions and assignment of the labeled peaks in the emission spectrum at 4 K for K_2LiAlF_6:Cr^{3+}, shown in Fig. 3

Line	Wavelength (nm)	Vibrational energy (cm^{-1})	Assignment
1	664.7	—	Zero-phonon line
2	668.6	87	Lattice phonon modes
3	670.1	121	Lattice phonon modes
4	671.3	148	Lattice phonon modes
5	674.7	223	$t_{2u}(\pi)$
6	676.2	256	$t_{2g}(\pi)$
7	678.3	301	$t_{1u}(\pi)$
8	681.5	370	$t_{2u}(\pi)+148$
9	684.1	426	$t_{1u}(\pi)+120$
10	686.2	471	$e_g(\sigma)$
11	690.4	560	$a_{1g}(\sigma)$
12	692.2	597	$t_{1u}(\sigma)$
13	697.1	699	$t_{2u}(\pi)+e_g(\sigma)$
14	701.4	787	$t_{2u}(\pi)+a_{1g}(\sigma)$
15	705.3	866	$t_{2u}(\pi)+a_{1g}(\sigma)+87$
16	708.1	922	$t_{2u}(\pi)+a_{1g}(\sigma)+148$
17	709.8	956	$t_{2u}(\pi)+e_g(\sigma)+t_{2g}(\pi)$
18	713.1	1021	$e_g(\sigma)+a_{1g}(\sigma)$
19	718.2	1120	$2a_{1g}(\sigma)$
20	725.2	1255	$2e_g(\sigma)+t_{1u}(\pi)$
21	728.4	1315	$t_{2u}(\pi)+2a_{1g}(\sigma)$
22	732.8	1398	$3e_g(\sigma)$
23	739.0	1512	$2e_g(\sigma)+t_{1u}(\pi)+t_{2g}(\pi)$
24	742.8	1582	$e_g(\sigma)+2a_{1g}(\sigma)$
25	749.3	1698	$3a_{1g}(\sigma)$
26	753.4	1771	$3a_{1g}(\sigma)+87$
27	763.9	1953	$3a_{1g}(\sigma)+t_{2g}(\pi)$

The energies of vibrational modes are relative to that zero-phonon line.

Table 2
Low temperature experimental energy positions and assignment of vibrational modes relative to $^4T_2(^4F) \rightarrow {}^4A_2(^4F)$ zero-phonon line to Cr^{3+} in fluorides hosts, in cm^{-1}

Assignments	K_2LiAlF_6	Cs_2NaScF_6	K_2NaScF_6	K_2NaGaF_6
$^4T_2 \rightarrow {}^4A_2$	15,044	13,875	14,549	15,041
$t_{2u}(\pi)$ bend	221	224	207	200
$t_{2g}(\pi)$ bend	254	—	—	234
$t_{1u}(\pi)$ bend	300	302	316	329
$e_g(\sigma)$ stretch	469	405	449	481
$a_{1g}(\sigma)$ stretch	558	506	572	568
$t_{1u}(\sigma)$ stretch	596	584	—	595

$^4T_2(^4F) \rightarrow {}^4A_2(^4F)$ transition corresponds to the zero phonon line in their vibronic spectra [2,26,27].

The excitation and absorption spectra of K_2LiAlF_6:Cr^3: 1% Cr^{3+} at room temperature are shown in Fig. 4(a) and (b), respectively. The sample is light green, therefore the attainment of absorption spectrum is very difficult. In the excitation spectrum, the band with barycenter at 436 nm is associated with $^4A_2(^4F) \rightarrow {}^4T_1(^4F)$ transition, while the band at 624.0 nm is attributed to $^4A_2(^4F) \rightarrow {}^4T_2(^4F)$ transition. The comparison between the energy position of the $^4T_2(^4F)$—$^4A_2(^4F)$ room temperature excitation and emission bands leads to a Stokes shift of 2420 cm^{-1}, a reasonable value for fluoride hosts [28]. We can extract the cubic field splitting parameter $10Dq$ from the barycenter of band energy associated with $^4A_2(^4F) \rightarrow {}^4T_2(^4F)$ transition. By Tanabe–Sugano matrices for Cr^{3+} ($3d^3$) in octahedral environment [5], the $^4A_2(^4F)$–$^4T_2(^4F)$ energy value is $10Dq$ and the crystal field parameter is ~1608 cm^{-1} [5]

$$\frac{B}{Dq} = \frac{(\Delta E/Dq)^2 - 10(\Delta E/Dq)}{15(\Delta E/Dq - 8)} \quad (1)$$

and from the energy difference ΔE between $^4A_2(^4F) \rightarrow {}^4T_1(^4F)$ and $^4A_2(^4F) \rightarrow {}^4T_2(^4F)$ transitions and with the crystal field parameter Dq value, we obtain the Racah parameter B~710 cm^{-1}. The Dq/B~2.3 value indicates that the $^4T_2$ and ^2E states are very close in energy, leading to intense e_g and a_{1g} modes [24]. Through the Racah B and crystal field Dq parameters and the $^4A_2(^4F) \rightarrow {}^4T_1(^4F)$ transition, we can estimate the energy position of $^4T_1(^4P)$ level as follows [21]:

$$^4T_1(^4P) - {}^4T_1(^4F) = [(9B - 10Dq)^2 + 144B^2]^{1/2}. \quad (2)$$

From this procedure a $^4T_1(^4P)$ level position at 283.0 nm is obtained. This value is in accord with expected values obtained from Tanabe–Sugano diagrams [21] of octahedrally coordinated Cr^{3+} ions in intermediate crystalline fields. According to Ref. [5], for $1.5 < Dq/B < 3.5$ values the Racah parameter C can be obtained from Eq. (3) with

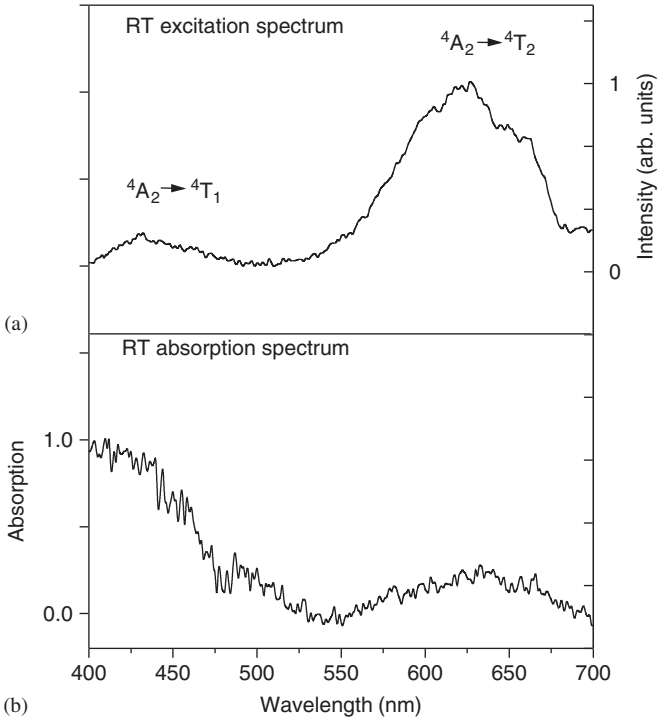

Fig. 4. Room temperature (a) excitation and (b) absorption spectra of K_2LiAlF_6 doped with 1.0 at% Cr^{3+}. The higher and lower energy bands are identified with $^4A_2(^4F) \rightarrow {}^4T_1(^4F)$ and $^4A_2(^4F) \rightarrow {}^4T_2(^4F)$ transition, respectively.

0.5% of relative accuracy as compared to the value obtained by matrices diagonalization:

$$\frac{E(^2E)}{B} \cong \frac{3.05C}{B} + 7.90 - 1.80\frac{B}{Dq}. \quad (3)$$

In Eq. (3), $E(^2E)$ is the energy of $^2E(^2G)$ level, associated with the dip in the excitation spectrum located at 657.0 nm, therefore below the $^4T_2(^4F)$ energy level. Since for the K_2LiAlF_6:Cr^{3+} sample the Dq/B value is approximately 2.3, we can extract the Racah parameter $C = 3341\ cm^{-1}$. For the free ions the Racah B and C parameters are associated with Coulomb repulsion of electrons. In crystals, these parameters are a measure of bond covalence between the ligand anions and the metal cations. The ratio $C/B = 4.7$ obtained for K_2LiAlF_6:Cr^{3+} is very close to those of other Cr^{3+} systems [2,27–30]. The ^2E–$^4T_2$ energy level separation of 800 cm^{-1} is small and the states remain in thermal equilibrium. The $^4T_2$ level is thermally populated only by non-radiative transitions out of the $^4T_1(^4F)$ states, because we have not found evidence of $^4T_1(^4F) \rightarrow {}^4T_2$ (^4F) luminescence. By the way, the assignments in excitation spectrum are coherent with luminescence attributions. In Fig. 4(b) we show the optical absorption at room temperature. We can identify two bands in the spectrum, associated with Cr^{3+} octahedrally coordinated. The barycenter of the highest energy band, associated with $^4A_2(^4F) \rightarrow {}^4T_1(^4F)$ transition, is not identified due to a poor response of experimental apparatus in

the higher energy region, while the band at 630.0 nm is attributed to $^4A_2\ (^4F) \rightarrow {}^4T_2(^4F)$ transition. We can observe that the incident wavelengths at red region are weakly absorbed in the sample, but are responsible by a higher photoluminescence intensity. Therefore, the possibility of diode lasers $K_2LiAlF_6:Cr^{3+}$ luminescence pumping turns this sample very interesting because those lasers are cheap and common devices. In our analysis we have not considered the energy transfer between the Cr^{3+} ions, because due to the low concentration of impurities in host crystal we believe that these processes can be neglected.

4. Conclusions

The photoluminescence, excitation and absorption of K_2LiAlF_6 doped with 1.0 at% of Cr^{3+} were investigated in this report. With the assumption that the chromium ions are occupying only one kind of site and using the Tanabe–Sugano energy matrices for a d^3 ion in cubic field, a crystal field $Dq = 1608\,cm^{-1}$ and Racah $B = 710\,cm^{-1}$ and $C = 3341\,cm^{-1}$ parameters were determined from room temperature excitation spectrum. Using the above calculated set of parameters the higher-energy transition $^4A_2(^4F) \rightarrow {}^4T_1(^4P)$ expected for the octahedrally coordinated Cr^{3+} ions to the F^- ions in the host lattice was calculated to be at 283 nm, which lies beyond our instrument capabilities.

The photoluminescence spectra show broad vibronic bands between 650 and 850 nm. Only one luminescence lifetime was detected in low-temperature through phase-shift measurements, indicating that in K_2LiAlF_6 the Cr^{3+} ion occupies one type of octahedral site. The absorption spectra show that an intensity of the $^4T_1(^4F)$ level is higher than that of the $^4T_2(^4F)$ level. We conclude that $^4T_2\ (^4F)$ level is populated by non-radiative transitions from $^4T_1(^4F)$, favoring the $^4T_2(^4F) \rightarrow {}^4A_2\ (^4F)$ emission. The normal vibrational modes of the octahedral complex $[CrF_6]^{3-}$ generate the analyzed spectrum, in which vibronic lines were ascribed to progressions of the local e_g and a_{1g} modes. The weaker lines in spectrum, as expected, are superposition of two or more local vibrational modes or also host vibrations.

It is important to remember that development of optical materials for applications as new devices or as more efficient materials for traditional applications is always interesting. Considering that the quantum efficiency of $K_2LiAlF_6:Cr^{3+}$ is about 0.6% and 10% of the 4 K emission intensity remains at room temperature, the study of this new Cr^{3+}-doped material for laser application is suitable.

Acknowledgments

We are grateful to FAPERJ, CNPq and FINEP for financial support and to N.M. Khaidukov, from the Institute of General and Inorganic Chemistry, Moscow, Russia, for providing the single crystal materials.

References

[1] S. Kück, Appl. Phys. B 72 (2001) 515–562.
[2] G.R. Wein, D.S. Hamilton, U. Sliwczuk, A.G. Rinzler, R.H. Bartram, J. Phys.: Condens. Matter 13 (2001) 2363–2375.
[3] O.S. Wenger, H.U. Güdel, J. Chem. Phys. 114 (2001) 5832–5841.
[4] T. Ohtake, N. Sonoyama, T. Sakata, Chem. Phys. Lett. 318 (2000) 517–521.
[5] B. Henderson, G.F. Imbusch, Optical Spectroscopy of Inorganic Solids, Clarendon Press, Oxford, 1989.
[6] S.T. Lai, J. Opt. Soc. Am. B 4 (1987) 1286–1290.
[7] S.A. Payne, L.L. Chase, H.W. Newkirk, L.K. Smith, W.F. Krupke, IEEE J. Quantum Electron. 24 (1988) 2243–2252.
[8] M. Stalder, B.H.T. Chai, M. Bass, Appl. Phys. Lett. 58 (1991) 216–218.
[9] A.A. Kaminskii, A.P. Shkadarevich, B.V. Mill, V.G. Kuptev, A.A. Demidovich, Inorg. Mater. 23 (1987) 618–619.
[10] R.J.M. da Fonseca, L.P. Sosman, A. Dias Tavares Jr., H.N. Bordallo, J. Fluoresc. 10 (2000) 375–381.
[11] D.R. Lee, T.P.J. Han, B. Henderson, Appl. Phys. A 59 (1994) 365–372.
[12] M. Mortier, Q. Wang, J.Y. Buzaré, M. Rousseau, B. Piriou, Phys. Rev. B 56 (1997) 3022–3031.
[13] S.M. Healy, C.J. Donnelly, T.J. Glynn, G.F. Imbusch, G.P. Morgan, J. Lumin. 46 (1990) 1–7.
[14] P. Hegenmuller, Inorganic Solid Fluorides, Chemistry and Physics, Academic Press, Orlando, FL, 1985.
[15] A. Tressaud, J. Darriet, P. Lagassié, J. Grannec, P. Hagenmuller, Mater. Res. Bull. 19 (1984) 983–988.
[16] P.A. Tanner, L. Yulong, N.M. Edelstein, K.M. Murdoch, N.M. Khaidukov, J. Phys.: Condens. Matter (1997) 7817–7836.
[17] Y. Tanabe, S. Sugano, J. Phys. Soc. Jpn. 9 (1954) 753–766.
[18] M. Yamaga, B. Henderson, K.P. O'Donnell, Phys. Rev. B 46 (1992) 3273–3282.
[19] L.P. Sosman, A.D. Tavares Jr., R.J.M. da Fonseca, T. Abritta, N.M. Khaidukov, Solid State Commun. 114 (2000) 661–665.
[20] R.J.M. da Fonseca, A.D. Tavares Jr., P.S. Silva, T. Abritta, N.M. Khaidukov, Solid State Commun. 110 (1999) 519–524.
[21] A.S. Marfunin, Physics of Minerals and Inorganic Materials, Springer, Berlin, 1979.
[22] C.M. de Lucas, F. Rodriguez, J.M. Dance, M. Moreno, A. Tressaud, J. Lumin. 48&49 (1991) 553–557.
[23] U. Sliwczuk, R.H. Bartram, D.R. Gabbe, B.C. McCollum, J. Phys. Chem. Solids 52 (1991) 357–361.
[24] P. Greenough, A.G. Paulusz, J. Chem. Phys. 70 (1979) 1967–1972.
[25] M.O. Ramirez, D. Jaque, M. Montes, J. Garcia Solé, L.E. Bausá, Appl. Phys. Lett. 84 (2004) 2787–2789.
[26] L.P. Sosman, R.J.M. da Fonseca, A. Dias Tavares Jr., M.K.K. Nakaema, H.N. Bordallo, J. Fluoresc. 16 (2006) 317–323.
[27] J.F. Dolan, A.G. Rinzler, L.A. Kapper, R.H. Bartram, J. Phys. Chem. Solids 53 (1992) 905–912.
[28] U.R. Rodríguez-Mendoza, A. Speghini, D. Jaque, M. Zambelli, M. Bettinelli, J. Alloys Compd. 380 (2004) 163–166.
[29] K. Hermanowicz, M. Mączka, M. Wołcyrz, P.E. Tomaszewski, M. Paściak, J. Hanuza, J. Solid State Chem. 179 (2006) 685–695.
[30] K.P. O'Donnell, A. Marshall, M. Yamaga, B. Henderson, J. Lumin. 42 (1989) 365–373.